Computational Materials Science 102 (2015) 21–26

Contents lists available at ScienceDirect

Computational Materials Science

journal homepage: www.elsevier.com/locate/commatsci

Phase transition and thermodynamic properties of YAg alloy from first-principles calculations

Chunying Pu [a], Dawei Zhou [a,*], Yuling Song [a], Zhuo Wang [a], Feiwu Zhang [b,c], Zhiwen Lu [a]

[a] College of Physics and Electronic Engineering, Nanyang Normal University, Nanyang 473061, China
[b] State Key Laboratory of Ore Deposit Geochemistry, Institute of Geochemistry, Chinese Academy of Sciences, Guiyang 550002, China
[c] Nanochemistry Research Institute, Curtin University, Perth, WA 6845, Australia

ARTICLE INFO

Article history:
Received 22 November 2014
Received in revised form 30 January 2015
Accepted 8 February 2015
Available online 27 February 2015

Keywords:
Phase transition
First-principles calculations
Thermodynamic properties

ABSTRACT

Using the particle swarm optimization algorithm on crystal structure prediction, we first predicted that YAg alloy undergoes a first-order phase transition from CsCl phase to Fd-3m phase at about 25 GPa with a volume collapse of 7.47%. An abrupt change of the electrical resistance was discovered accompanying the phase transformation. Our results showed that external pressure has different effects on the ductility and anisotropy of the two phases. External pressure can improve the ductility of CsCl phase, while it has a negligible effect on that of Fd-3m phase. As pressure increases, the elastic anisotropy of CsCl phase increases rapidly, while that of Fd-3m phase remains unchanged. The structural stability, electronic structure, and thermodynamic properties of the two phases under pressure were also investigated systematically.

1. Introduction

Rare-earth intermetallic compounds have received great attention due to their unique mechanical and physical properties, such as high strength and stiffness, low specific weight corrosion resistance, and hot strength superior to ordinary metals [1,2], However, their poor fracture toughness and brittleness at room temperature restrict their applications [3]. In recent years, a new large family rare earth intermetallics (e.g. YAg, YCu, CeAg, HoCu, NdAg) has been discovered at room temperature [3,4]. Those compounds are known to crystallize in a cubic lattice of CsCl-type structure (B2) with the space group Pm-3m (221). In particular, they have remarkably high ductility, low unstable stacking fault energies, and an unusual relationship between the Poisson ratio and the elastic anisotropy. Among the discovered intermetallic compounds, YAg alloy is found to be the most ductile rare-earth intermetallic compound, in some cases exceeding 20% ductility in tension [5]. Many theoretical and experimental works [6–13] have been done to understand the mechanism of high ductility for YAg at room temperature, such as elasticity, phase stability, dislocation mechanisms, thermodynamic properties, electronic structure and density of states. To get better understanding of the ductility of YAg, temperature dependent properties such as thermal expansion, heat capacity and thermoelasticity have also been investigated [14]. Up to now, the properties of YAg alloy with B2-type structure under ambient pressure have been systematically studied and clear, but those under high pressure have not been investigated. It is well known that pressure could effectively alter their electronic bonding states to modify the physical properties or induce the formation of new structure, thus pressure provides a perfect tool to change the electronic and structural properties of materials in a controlled manner. Therefore, it is desirable to explore the high-pressure phases of YAg alloy and the mechanical properties might be fundamentally revised.

The main purpose of this work is to help in designing and understanding the high-pressure behavior of YAg alloy. Using the particle swarm optimization algorithm, we first explore the high-pressure phases of YAg alloy, then study the pressure influences on the properties of YAg alloy. The structural stability, electronic structure, and thermodynamic properties of YAg alloy under pressure are investigated systematically in this paper.

2. Computational methods

The crystal structure prediction is based on a global minimization of enthalpy surfaces merging *ab initio* total energy calculations as implemented in the Crystal structure analysis by Particle Swarm Optimization (CALYPSO) code in the pressure range 0–100 GPa [15,16], which has been successfully applied to predict high pressure structures [17–19]. The structural relaxations used projector

* Corresponding author.
E-mail address: zhoudawei@nynu.edu.cn (D. Zhou).

http://dx.doi.org/10.1016/j.commatsci.2015.02.011
0927-0256/

augmented wave (PAW) method [20] as implemented in the Vienna *ab initio* simulation package (VASP) [21]. Ag-4d, 5s and Y-4s, 4p, 4d, 5s electrons as valence band are adopted. The exchange-correlation energy was treated within the generalized gradient approximation (GGA), using the functional of Perdew et al. [22]. The cutoff energy of 600 eV and Monkhorst-Pack *k*-point spacing of $2\pi \times 0.03$ Å^{-1} were chosen to ensure that enthalpy calculations are well converged to better than 1 meV/atom. The phonon calculations were calculated with a supercell approach as implemented in the PHONOPY program [23]. Convergence check gave the use of a $2 \times 2 \times 2$ supercell with a total of 128 atoms and $4 \times 4 \times 4$ *k*-meshes for the Fd-3m structure. In this work, stress–strain method was used to evaluate the elastic constants of YAg [24].

3. Results and discussion

We first calculated the structural properties of CsCl phase at 0 GPa. The calculated structural parameters, elastic stiffness constants, bulk modulus *B*, shear modulus *G* and the ratio of *G*/*B* are listed in Table 1. The calculated values are in good agreement with the experimental values and previous theoretical results [5,25,26], indicating that our calculations are valid and believable.

To explore the high-pressure phases of YAg alloy, variable-cell simulations with 1–8 formula units (f.u.) in the unit cell were performed at 0, 10, 50 and 100 GPa, respectively. The ambient-pressure phase of CsCl structure was correctly predicted at zero pressure. At higher pressures, our structural prediction revealed an energetically favorable cubic structure with space group Fd-3m (No. 227) containing 4 f.u./unit cell, the conventional cell of which is shown in Fig. 1. In order to determine the structural phase-transition sequence of YAg alloy, the enthalpy curves of the Fd-3m structure and the competitive structures of B_2 alloy [27] with respect to the CsCl structure as a function of pressure is shown in Fig. 1. Although the competitive structures of B_2 phase in Al–RE (RE = rare earth elements) alloys are energetically lower than B2 structure at 0 GPa, it is found that the CsCl structure is the most stable for YAg alloy. The structural transition pressure from CsCl to Fd-3m phase is predicted at 25 GPa. The Fd-3m phase at 25 GPa has the optimized lattice parameter: $a = 6.031$ Å and Wyckoff position sites of Y 48f (0.5, 0.0, 0.0), Ag 32e (0.25, 0.25, 0.25). The *P*–*V* relation of CsCl and Fd-3m for YAg is also plotted in Fig. 1. It can be seen that there is about 7.47% volume collapse accompanying the structural transition, indicating that Fd-3m structure is more compressible than the CsCl structure and the occurrence of first order phase transition.

To further check the dynamical stability of Fd-3m phase, the phonon dispersion curves and partial phonon density of states (DOS) at 25 GPa are shown in Fig. 2. As seen from the phonon dispersion curves, no negative frequency have been found, implying the Fd-3m phase is dynamically stable. In Fig. 2, we also plot the partial phonon DOS with *i* = (Y, Ag), respectively. The peaks at whole frequencies region are composed of states of Y atom and

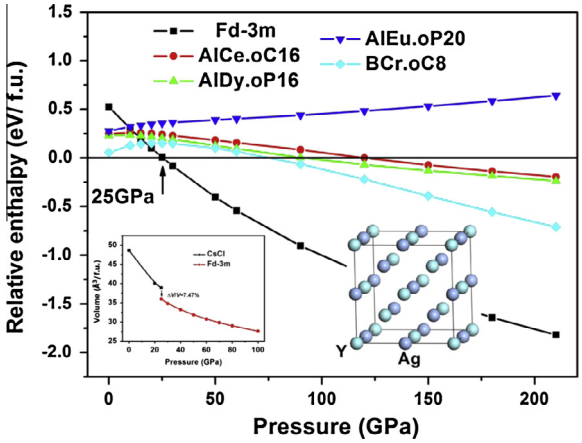

Fig. 1. The enthalpy difference between Fd-3m and CsCl structure versus pressure. The inset is the pressure versus volume for YAg alloy.

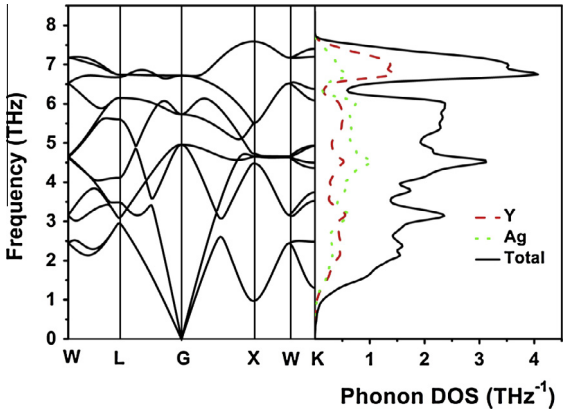

Fig. 2. Calculated phonon dispersion curves and vibrational DOS (black solid line) for Fd-3m structure of YAg at 25 GPa, along with partial DOS from Y (red dotted line) and Ag (green dashed line). (For interpretation of the references to colour in this figure legend, the reader is referred to the web version of this article.)

Ag atom. At high frequencies (about above 6.3 THz), the phonon DOSs mainly come from the Y atoms. At middle frequencies (about 2.85–6.35 THz), the contribution from Y is lower than that of Ag. However, at low frequency (about below 2.9 THz), the contribution from Y is higher than that of Ag again. Unfortunately, there are no experimental data and theoretical results on the lattice dynamics of this compound at high pressure in literature for comparison with the present ones.

To study the electrical characteristics of the YAg at high pressure, the partial and total DOS for CsCl and Fd-3m structures at 25 GPa are shown in Fig. 3a and b, respectively. It is found that the metallic character in both the structures is mainly due to the

Table 1
The calculated parameters *a* (Å), elastic constants (GPa), bulk modulus *B* (GPa), shear modulus *G* (GPa) and the ratio of *G*/*B* for CsCl phase compared with previous theoretical results at zero pressure.

	a	C_{11}	C_{12}	C_{44}	*B*	*G*	*G*/*B*
CsCl (this work)	3.651	93.8	48.9	34.4	63.9	29.0	0.454
Previous work	3.64[a]	97.15[a]	49.7[a]	32.049[a]	65.52[a]	28.41[a]	0.435[a]
	3.64[b]	98.3[b]	53.5[b]	33.6[b]	68.4[b]	28.26[b]	
Experiment	3.61[c]	102.4[c]	54.0[c]	37.2[c]	70.5[c]	28.9[d]	0.412[d]

[a] Ref. [12].
[b] Ref. [25].
[c] Ref. [5].
[d] Ref. [26].

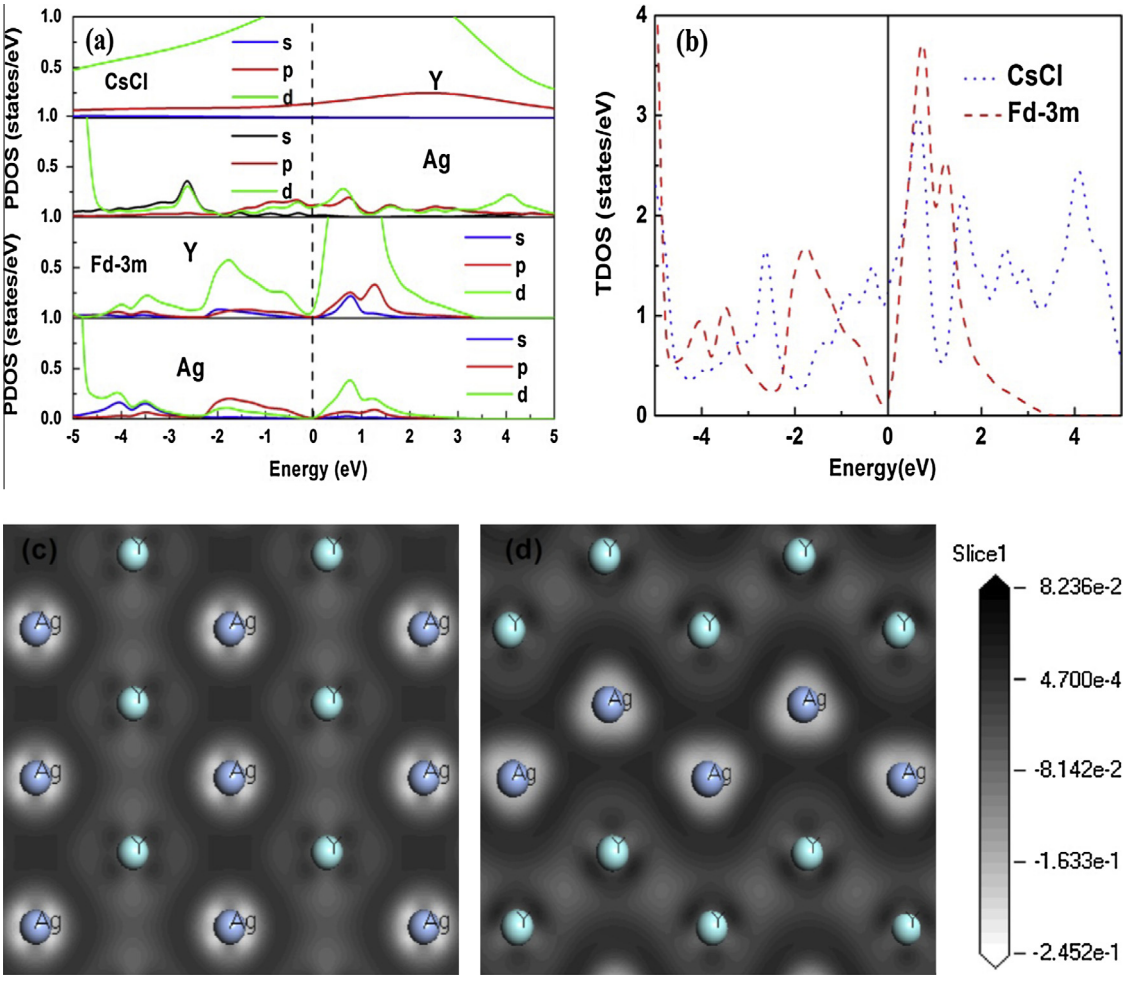

Fig. 3. The partial (a) and total (b) density of states for CsCl phase and Fd-3m phase at 25 GPa, and electronic charge density difference contour plots on different planes: (c) CsCl phase (d) Fd-3m phase.

contribution from Y-d states to the DOS at Fermi level. Moreover, Fd-3m structure has lower total DOS at the E_F than that of CsCl structure at 25 PGa, indicating that the Fd-3m structure is a stable phase. The DOS at E_F for the Fd-3m structure is smaller by almost 62% compared to that of CsCl phase. This substantial decrease in the total DOS at the E_F during the phase transition would imply much larger electrical resistance; therefore we believe that there is an abrupt change in the electrical resistance accompanying the CsCl-to-Fd-3m phase transformation. In order to gain more insight into the bonding nature of YAg at 25 GPa, we also investigate the electron charge density maps, which are defined as the electron density difference between the isolated atoms and their bonding states, directly reflect their bonding nature. The electron charge density difference distributions of two structures of YAg at 25 GPa on the different plane are shown in Fig. 3. The contour lines are plotted from -0.2452 to 0.08236 eV/Å^3. The dark lines correspond to higher density region, and the gray lines correspond to lower density region. From Fig. 3(c) and (d), it is found that there are ionic Y–Ag bonds, covalent Ag–Ag bonds and metallic Y–Y bonds in both structures. However, the charge accumulation along Y–Ag bond is smaller than that along the Ag–Ag bond. According to analysis of densities of states (DOS) and the electronic charge density difference, Fd-3m structure has the strongest structure stability because of the strong covalent bonds combined action.Using the pressure dependence of elastic constants, one can judge the mechanical stability of a crystal structure under high pressure. Pressure dependence of all elastic constants of CsCl and Fd-3m phases are shown in Fig.4. There are 3 independent elastic constants (C_{11}, C_{12}, and C_{44}) for the cubic structure. The criteria for mechanical stability [28] are presented as $C_{11} > 0, C_{44} > 0, C_{11} > |C_{12}|, C_{11} + 2C_{12} > 0$. It is found that CsCl phase is mechanical stable until pressure 52 GPa. After that, C_{11} is smaller than C_{12},

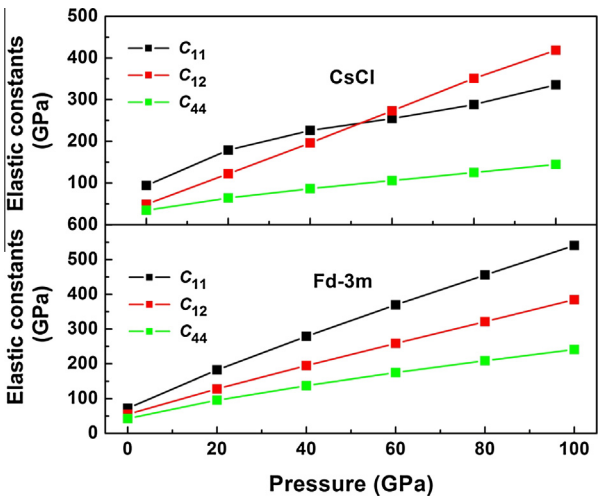

Fig. 4. Calculated elastic constants of C_{11}, C_{12}, and C_{44} for YAg with pressure in CsCl and Fd-3m structures.

suggesting the elastic instability at pressure above 52 GPa. Moreover, the new predicted Fd-3m phase meets the mechanical stable conditions in the whole pressure range studied.

Once the single-crystal elastic constants C_{ij} are obtained, one can estimate many other important macroscopic mechanical parameters. For example, the isotropic aggregate bulk modulus B and shear modulus G can be obtained from elastic constants using the Voigte ReusseHill (VRH) approach according to the following formula [29–32]:

$$B_V = B_R = (C_{11} + 2C_{12})/3 \tag{1}$$

$$G_V = (C_{11} - C_{12} + 3C_{44})/5 \tag{2}$$

$$G_R = 5(C_{11} - C_{12})C_{44})/4[C_{44} + 3(C_{11} - C_{12})] \tag{3}$$

$$B = (B_V + B_R)/2, \quad G = (G_V + G_R)/2 \tag{4}$$

Moreover, Debye temperature Θ_D at low temperatures is proportional to the sound velocity and also related to the elastic constant through bulk and shear moduli [32]:

$$\Theta_D = \frac{h}{k_B}\sqrt[3]{\frac{3nN_A\rho}{4\pi M}}v_m \tag{5}$$

where h is Planck's constant, k_B is Boltzmann's constant, n is the number of atoms per formula unit, M is the molecular weight, N_A is Avogadro's number, ρ is the density and v_m is the average sound velocity. In fact, v_m can be obtained from the longitudinal wave velocities v_l and transverse wave velocities v_s

$$\frac{3}{v_m^3} = \frac{1}{v_l^3} + \frac{2}{v_s^3}, \quad v_l = [(B + 4/3G)/\rho]^{1/2}, \quad v_s = (G/\rho)^{1/2} \tag{6}$$

The calculated bulk and shear moduli, Debye temperatures and G/B ratio under pressure for both phases are shown in Fig. 5. It can be seen that the pressure has important influences on the bulk modulus, shear modulus as well as Debye temperature. The bulk modulus of YAg in both phases increase linearly in the similar slope when the pressure is enhanced, where the shear modulus exhibit different behavior. The variation of shear modulus in Fd-3m phase increases linearly with increasing pressure, whereas that of CsCl phase is initially increasing firstly and then decreasing. The variation of Debye temperature has the same tendency with shear modulus, revealing that the shear modulus play a dominated role on Debye temperature according to the formula (5) and (6).

Since CsCl phase at room conditions is found to be the most ductile rare-earth intermetallic compound, we further to investigate the pressure effect on the ductile behavior. In fact, the ratio of shear modulus to bulk modulus (G/B) has been proposed by Pugh [33] to roughly estimate brittle or ductile behavior of materials. A lower G/B ratio denotes better ductility, and the critical value which separates ductility from brittleness is about 0.57. As can be seen from Fig. 5, G/B ratio are all smaller than 0.57 for both structures, which means that both phases behave in a ductile manner in the whole pressure range studied. However, G/B ratio of CsCl phase decreases with pressure, indicating the degree of ductility of CsCl phase increases under pressure. Interestingly, the G/B ratio of Fd-3m phase remains nearly unchanged with increasing pressure. Therefore pressure has a negligible effect on the ductility of Fd-3m phase.

We further to examine the pressure effects on the anisotropy of the two phases. A concept of percentage elastic anisotropy which is a measure of elastic anisotropy possessed by the crystal is proposed by Chung and Buessem [34]. The percentage anisotropy in compressibility and shear are given by

$$A_B = \frac{B_V - B_R}{B_V + B_R}, \quad A_G = \frac{G_V - G_R}{G_V + G_R} \tag{7}$$

where B and G are the bulk and shear modulus, and the subscripts V and R represent the Voigt and Reuss approximation. It is well known that, if all of the indexes in Eqs. (1) and (2) are zero, the structure is isotropic. The larger deviations from zero imply the higher anisotropic mechanical properties. Fig. 6 shows the pressure dependence of results. For both structures, we can see that the anisotropy factor A_B is zero on the whole pressure range we investigated, indicating a complete elastic isotropy in compressibility. However, the anisotropy factor A_G of both phases is larger than zero and exhibits different behavior under pressure. Specially, the anisotropy factor A_G of CsCl increases rapidly with pressure, while that of Fd-3m phase remains constant above 25 GPa.

The universal anisotropic index (A^U) is a better indicator than other indices and can be written as: [35]

$$A^U = 5\frac{G_V}{G_R} + \frac{B_V}{B_R} - 6 \geqslant 0 \tag{8}$$

The larger the value of A^U is, the stronger the anisotropy of the compound. It can be easily seen that with increasing pressure, A^U of Fd-

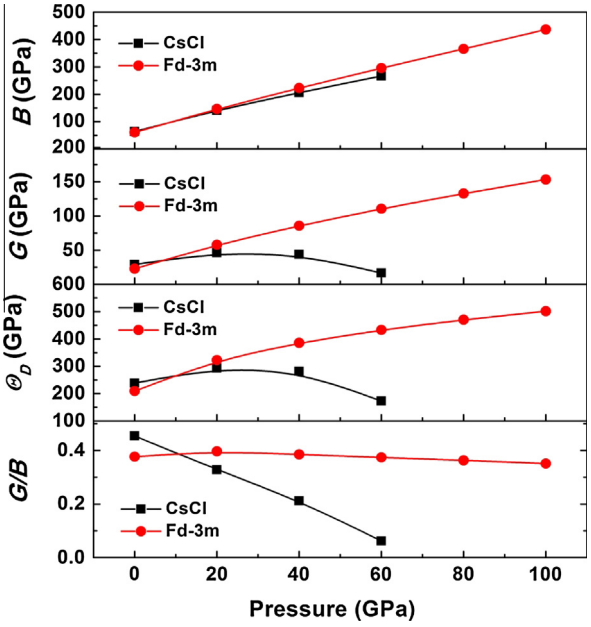

Fig. 5. Pressure dependence of bulk modulus B, shear modulus G, Debye temperature Θ_D and G/B ratio of YAg.

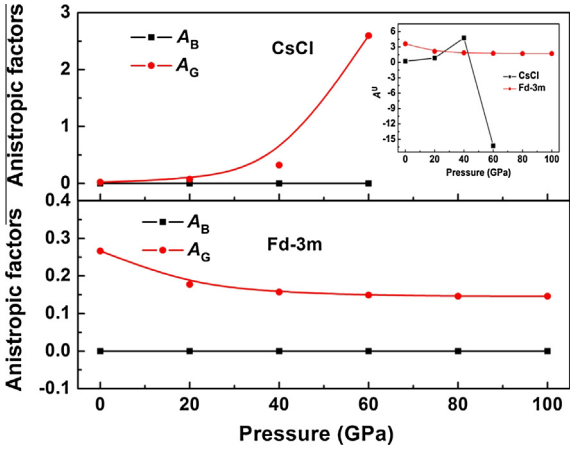

Fig. 6. Pressure dependence of percent anisotropy A_B and A_G and the universal anisotropic index A^U (inset) for YAg alloy.

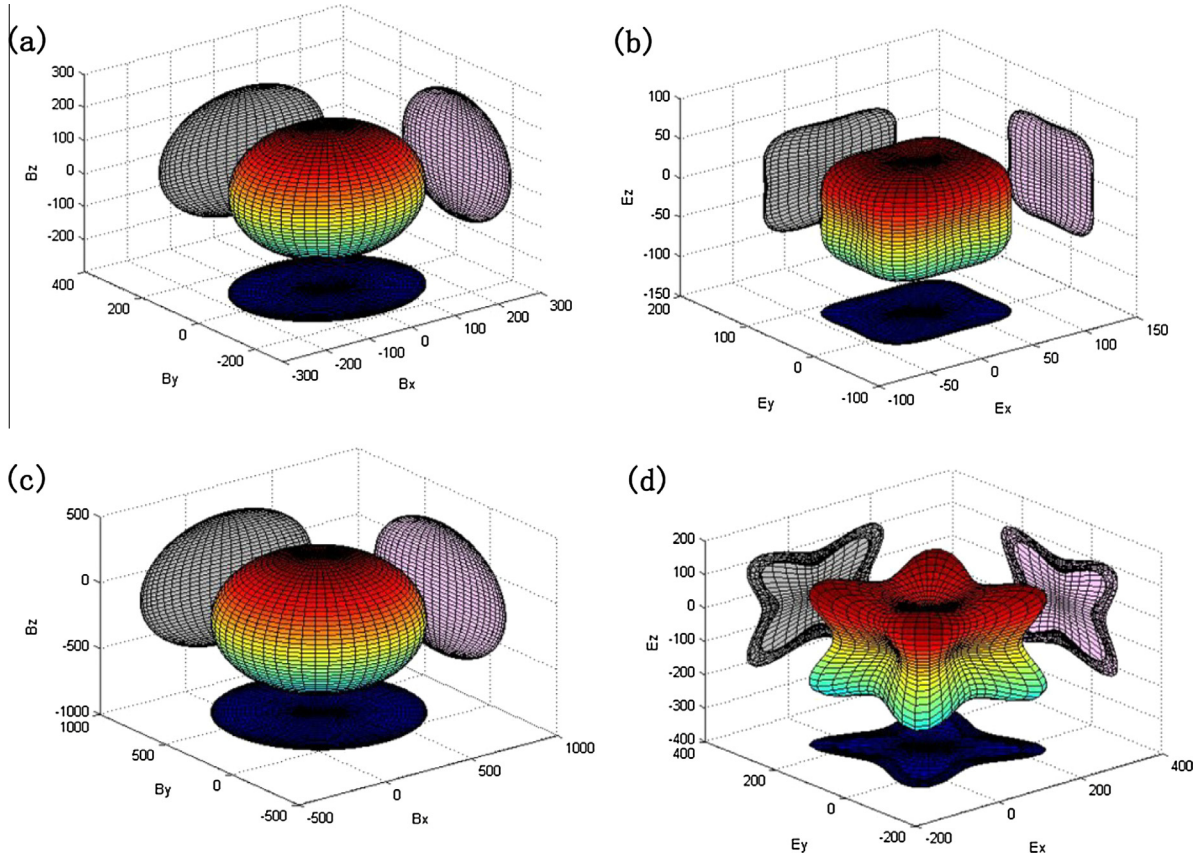

Fig. 7. The surface constructions and planar projections of bulk modulus (a) and Young's modulus (b) for CsCl phase at 0 GPa. The surface constructions and planar projections of bulk modulus (c) and Young's modulus (d) for Fd3 m phase at 25 GPa.

3m phase remains constant, while that of CsCl phase increases rapidly. Therefore, we can conclude that the anisotropy in CsCl phase increases with pressure, while that of Fd-3m phase remains nearly unchanged.

As we know, the elastic anisotropy of a crystal can be characterized by many different ways. As another valid method to describe the elastic anisotropic constructions of the directional dependences of reciprocals of bulk modulus and Young's modulus are practically useful. We have built a curved surface of a three dimensional (3D) to state the elastic anisotropy of crystal structure on crystallographic directions. For cubic system [36],

$$\frac{1}{B} = S_{11} + 2S_{12} \tag{9}$$

$$\frac{1}{E} = S_{11} - 2\left(S_{11} - S_{12} - \frac{S_{44}}{2}\right)\left(l_1^2 l_2^2 + l_2^2 l_3^2 + l_1^2 l_3^2\right) \tag{10}$$

where S_{ij} is the usual elastic compliance constant, which is obtained from the inverse of the matrix of the elastic constants. l_1, l_2 and l_3 are the direction cosines. The bulk modulus and Young's moduli of YAg in CsCl phase at 0 GPa and Fd-3m phase at 25 GPa are shown in Fig. 7. For an isotropic system, the 3D directional dependence would exhibit a spherical shape, while the deviation degree from the spherical shape reflects the content of anisotropy. From Fig. 7 we can see that the 3D figures of the bulk modulus for CsCl phase at 0 GPa and Fd-3m phase at 25 GPa have almost no deviation in shape from the sphere, which indicates that the bulk modulus show a smaller anisotropy. However, we obviously find that YAg compounds show a strong anisotropic character in Young's modulus, especially for Fd-3m structure. The projections on the (010), (100), and (001) planes show more details about the anisotropic properties of Young's modulus as shown in Fig. 7. It can be seen that Young's modulus of Fd-3m phase has a stronger directional dependence on these planes. The planar contours in these three planes are similar, which implies the analogous anisotropy for Young's modulus.

4. Conclusions

In conclusion, a pressure-induced first-order phase transition of YAg alloy has been predicted by using a particle swarm optimization algorithm in crystal structural prediction. The structural phase transition was predicted at 25 GPa, and the high-pressure phase is identified to be Fd-3m structure. A Volume collapse and an abrupt change of the electrical resistance were found accompanying phase transformation. Furthermore, both phases behave in ductility under pressure. Interestingly, it is found that pressure can improve ductility of CsCl phase, while it has a negligible effect on the ductility of Fd-3m phase. As pressure increases, the elastic anisotropy in CsCl phase increases rapidly with pressure, while that of Fd-3m remain unchanged. Furthermore, both phases exhibit a complete elastic isotropy in compressibility. With pressure increasing, the anisotropy in shear for CsCl phase increases, while it is nearly unchanged for Fd-3m phase. The weak anisotropic character in bulk modulus and strong anisotropic character in Young's modulus were also found in both phases. The structural stability, electronic structure and elastic modulus as well as Debye temperature of two phases under pressure were also discussed in details in this paper. In fact, there are 120 B2 alloys reported, the phase transition occurs in YAg alloy may occur in other B2 alloys. We suggest that further detailed experimental exploration of this phase transition may be rather rewarding.

Acknowledgements

The work is supported by the Henan Joint Funds of the National Natural Science Foundation of China (Grant Nos. U1304612, U1404608), National Natural Science Foundation of China (Grant No. 51374132), the Special Fund of the Theoretical Physics of China (Grant No. 11247222), and Feiwu Zhang acknowledges the support from the "Hundred Talent Program" of the Chinese Academy of Sciences (CAS).

References

[1] P. Lazar, R. Podloucky, Phys. Rev. B 73 (2006) 104114.
[2] P. Gumbsch, R. Schroll, Intermetallics 7 (1999) 447.
[3] K.A. Gschneidner Jr., A.M. Russell, A.O. Pecharsky, J.R. Morris, Z. Zhang, T.A. Lograsso, D.K. Hsu, C.H.C. Lo, Y. Ye, A.J. Slager, D.C. Kesse, Nat. Mater. 2 (2003) 587.
[4] K.A. Gschneidner Jr, M. Ji, C.Z. Wang, K.M. Ho, A.M. Russell, Y. Mudryk, et al., Acta Mater. 57 (2009) 5876.
[5] J.R. Morris, Y. Ye, Y.-B. Lee, B.N. Harmon, K.A. Gschneidner Jr., A. Russell, Acta Mater. 52 (2004) 4849.
[6] Z. Zhang, A.M. Russell, S.B. Biner, K.A. Gschneidner Jr., C.C.H. Lo, Intermetallics 13 (2005) 559.
[7] Q. Chen, S.B. Biner, Acta Mater. 53 (2005) 3215.
[8] A.M. Russell, Z. Zhang, T.A. Lograsso, C.C.H. Lo, A.O. Pecharsky, J.R. Morris, Y. Ye, K.A. Gschneidner Jr., A.J. Slager, Acta Mater. 52 (2004) 4033.
[9] S. Xie, A.M. Russell, A.T. Becker, K.A. Gschneidner, Scripta Mater. 58 (2008) 1066.
[10] Yurong Wu, Wangyu Hu, Shaochang Han, Physica B: Condens. Matter 403 (2008) 3792.
[11] S. Uğur, G. Uğur, F. Soyalp, R. Ellialtiğlu, J. Rare Earths 27 (2009) 664.
[12] A. Sekkal, A. Benzair, T. Ouahrani, H.I. Faraoun, G. Merad, H. Aourag, C. Esling, Intermetallics 45 (2014) 65.
[13] Rui Wang, Shaofeng Wang, Wu Xiaozhi, Intermetallics 18 (2010) 1653.
[14] Rui Wang, Shaofeng Wang, Xiaozhi Wu, Yin Yao, Physica B 406 (2011) 3951.
[15] Y.C. Wang, J. Lü, L. Zhu, Y.M. Ma, Phys. Rev. B 82 (2010) 094116.
[16] Y. Wang, J. Lv, L. Zhu, Y. Ma, Comput. Phys. Commun. 183 (2012) 2063.
[17] Lin Cui, Qianqian Wang, Bo Xu, Dongli Yu, Zhongyuan Liu, Yongjun Tian, Julong He, J. Phys. Chem. C 117 (2013) 21943.
[18] Yinwei Li, Quan Li, Yanming Ma, Europhys. Lett. 95 (2011) 66006.
[19] Hongbo Wang, Quan Li, Hui Wang, Hanyu Liu, Tian Cui, Yanming Ma, J. Phys. Chem. C 114 (2010) 8609.
[20] G. Kresse, D. Joubert, Phys. Rev. B: Condens. Matter Mater. Phys. 59 (1999) 1758.
[21] G. Kresse, J. Furthmüller, Phys. Rev. B 54 (1996) 11169.
[22] J.P. Perdew, K. Burke, M. Ernzerhof, Phys. Rev. Lett. 77 (1996) 3865.
[23] A. Togo, F. Oba, I. Tanaka, Phys. Rev. B: Condens. Matter Mater. Phys. 78 (2008) 134106.
[24] Y. Le Page, P. Saxe, Phys. Rev. B 65 (2002) 104104.
[25] X. Tao, H. Chen, X. Li, Y. Ouyang, S. Liao, Phys. Scr. 83 (2011) 045301.
[26] S.S. Chouhan, P. Soni, G. Pagare, S.P. Sanyal, M. Rajagopalan, Physica B 406 (2011) 339.
[27] Michael.C. Gao, Anthony.D. Rollett, Michael Widom, Phys. Rev. B 75 (2007) 174120.
[28] M. Bom, K. Huang, Dynamical Theory of Crystal Lattices, Clarendon, Oxford, 1954.
[29] I.R. Shein, A.L. IvanovskII, Scripta Mater. 59 (2008) 1099.
[30] I.R. Shein, A.L. IvanovskII, Physica C 469 (2009) 15.
[31] R. Hill, Proc. Phys. Soc. London A 65 (1952) 349.
[32] O.L. Anderson, J. Phys. Chem. Solids 24 (1963) 909.
[33] S.F. Pugh, Philos. Mag. Ser. 45 (1954) 823.
[34] D.H. Chung, W.R. Buessem, Anisotropy in Single Crystal Refractory Compound, Plenum Press, New York, 1968, p. 217.
[35] S.I. Ranganathan, M. Ostoja-Starzewski, Phys. Rev. Lett. 101 (2008) 055504.
[36] J.F. Nye, Physical Properties of Crystals: Their Representation by Tensors and Matrices, Oxford University Press, Great Britain, 1957.